Physical Modelling in Geotechnics – 6th ICPMG '06 – Ng, Zhang & Wang (eds)
© 2006 Taylor & Francis Group, London, ISBN 0-415-41586-1

In situ seismic monitoring during centrifuge tests of jacked piles

Y. Zhao, D.J. White & M.D. Bolton
Department of Engineering, University of Cambridge, U.K

ABSTRACT: Centrifuge tests simulating the installation of jacked piles were conducted in dense uniform fine silica sand. Seismic wave velocity distributions within the soil bed beneath and beside the pile were measured at various stages of pile penetration using accelerometer arrays and an air hammer vibration source. The pile penetration resistance and the concurrent variation of normalized G_0 are presented. Consistent trends of G_0 variation were observed and the local stress regime around the base and along the shaft was inferred. The observed stress distribution directly below the pile base is well-fitted by a cavity expansion analysis, and the stress distribution along the shaft provides evidence of friction fatigue and the conditions leading to set-up.

1 INTRODUCTION

The measurement of seismic velocity in situ is a simple method to characterize the ground. G_0 can be deduced from this velocity measurement, assuming the soil to be an isotropic elastic continuum. Seismic monitoring is often carried out in the field using a CPT equipped with seismic receivers and using bender elements in the laboratory. Knowledge of the G_0 distribution in situ provides a valuable stiffness parameter for design or numerical modelling. Variations in G_0 with wave orientation also give information on anisotropy due to soil fabric or stress.

This approach has potential value in the continuous monitoring of soil response to processes such as piling or grouting that can be expected to transform the surrounding soil properties or stress distributions during construction.

In piled foundations especially, the soil-structure interface governs the behaviour of the finished structure, yet the material and stress regime in this region is only created during the installation process. Accordingly, information on the changes of soil stiffness during construction provides valuable insight.

Pile jacking is one such construction process in which the use of continuous seismic monitoring can aid the understanding of pile base load-settlement behaviour and pile shaft resistance phenomena such as friction fatigue and set-up.

This paper presents seismic monitoring data during jacked pile installation. These tests were carried out on the 10 m diameter Turner beam centrifuge in the Schofield Centre at the University of Cambridge.

2 EXPERIMENTAL METHODOLOGY

2.1 *Piling actuator*

The pile jacking was conducted using an actuator with one vertical degree of freedom. The actuator is capable of exerting 10 kN of compression or tension while travelling at any speed up to 10 mm/s. The model pile is fixed to the actuator and the movement is logged continuously using a wire potentiometer, a linear variable differential transformer (LVDT) or a laser displacement sensor. The force applied at the top of the pile is recorded using a load cell. Figure 1 shows a typical model package for this type of experiment.

The original design and use of this actuator is described by Silva (2005). The current configuration used for pile jacking and a recent upgrade to computer feedback control are illustrated and described by Deeks & White (2006).

2.2 *Model pile and test sand*

The model pile is a straight thick-walled aluminium alloy tube of 12.7 mm outer diameter and 2 mm wall thickness. The pile was fitted with a strain-gauged load cell at the base to record the unit base load, which is denoted q_c, and is analogous to CPT tip resistance since the pile is closed-ended, albeit with a flat rather than conical tip.

The sand was recycled from previous centrifuge experiments that used commercial fine silica sand purchased from David Ball UK Ltd, which is identified as Fraction E silica sand. The new Fraction E sand has the following properties: $D_{10} = 0.095$ mm,

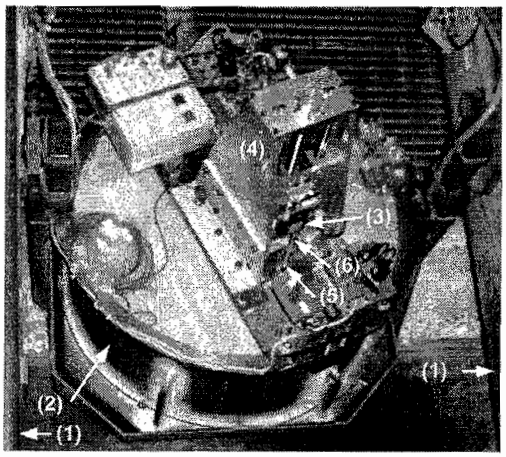

(1) Arms of beam centrifuge
(2) 850 mm diameter tub
(3) Laser displacement sensor
(4) Vertical actuator
(5) Model pile
(6) Vertical load cell

Figure 1. Centrifuge model package for jacked pile testing.

$D_{50} = 0.14$ mm, $D_{90} = 0.15$ mm, $\gamma_{max} = 1643$ kg/m^3, $\gamma_{min} = 1316$ kg/m^3 and $G_s = 2.65$ (Haigh & Madabhushi 2002). These previous experiments subjected the new Fraction E sand to repeated saturation and drainage, during which 9% (by mass) of the fines were lost. It is this modified Fraction E sand that is used in the experiments described in this paper.

2.3 *Soil model preparation*

Dry sand was poured into a steel tub of circular cross section, 850 mm diameter and 400 mm deep, using a robotic sand pourer. The pourer operates by discharging sand from a nozzle through multiple sieves and a controllable drop height to achieve uniform flow rates. Its construction and calibration are described separately in Madabhushi et al. (2006) and Zhao et al. (2006). For all the tests presented herein the sand bed was approximately 370 to 380 mm deep with a bulk density of 1643 kg/m^3; giving a relative density value of 100% if the maximum and minimum densities of non-modified Fraction E sand are used in the relative density calculation.

2.4 *Air hammers*

An air hammer is used as the source of vibration. The current design follows that of Ghosh (2004). It consists of a metal tube, within which a piston is propelled back and forth by pressurized air. Each time the piston travels the full length of the chamber it hits an end-stop and the impact produces a shock wave that travels in the plane of the cross section of the cylinder and vibrates in the direction parallel to the axis of the cylinder.

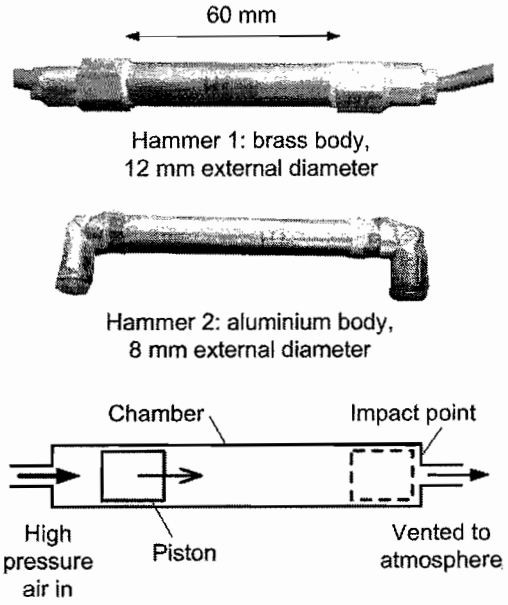

Figure 2. Air hammers.

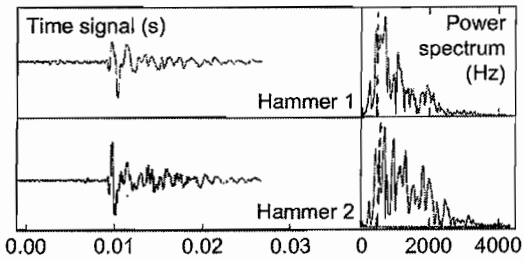

Figure 3. Typical shock waves as recorded by accelerometers.

Figure 2 shows the two air hammers used and their schematic construction. Figure 3 illustrates typical shock wave signals created by the hammers.

2.5 *Arrangement of accelerometer arrays*

The results from two types of accelerometer arrangements are presented herein (Figure 4). The air hammers and accelerometers are always excited in the same horizontal direction. The first arrangement involves four vertically spaced accelerometers which detect waves travelling vertically and vibrating in the horizontal direction (v_{vh}). An air hammer is located vertically below the accelerometers.

The second arrangement consists of four horizontally spaced accelerometers which detect waves traveling horizontally and vibrating in the horizontal direction (v_{hh}). A parallel air hammer is placed beyond the accelerometers. Figure 5 shows this arrangement

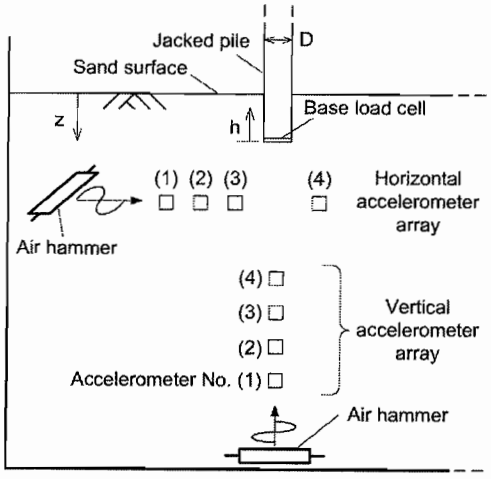

Figure 4. Horizontal cross-section of instrumentation layout.

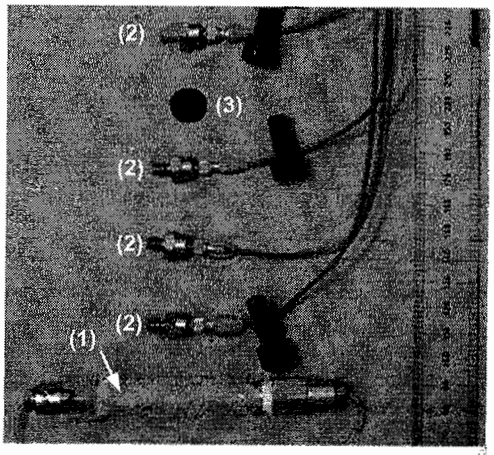

Figure 5. Plan view of horizontal accelerometer array and air hammer during model preparation.

during model preparation. The black solid circle indicates the position which is directly underneath the path of the pile during installation.

The accelerometers are numbered such that the one placed closest to the air hammer is given an identification (ID) number of (1), the second closest (2) and so forth.

2.6 *Accelerometer data processing*

Each pair of adjacent accelerometers registers a time difference in arrival of the same shock wave. This allows the average wave velocity of the soil between

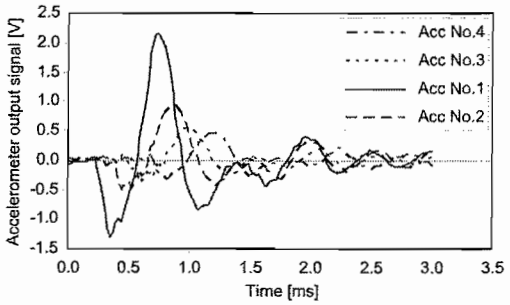

Figure 6. Typical accelerometer signals.

them to be derived. The average velocity associated with a particular pair of accelerometers is identified with subscripts of the ID numbers of that pair, e.g. $v_{hh\text{-}12}$ and $G_{0hh\text{-}12}$ for the average wave velocity and G_0 measured using accelerometer nos. 1 and 2.

Typical accelerometer signals exhibit pronounced peaks and troughs (Figure 6). For each pair of adjacent accelerometers, the time difference of the occurrence of the most significant peaks is determined by comparing signals using cross-correlation in the time domain. G_0 is then calculated as $G_0 = \gamma v^2$, from elastic wave theory.

2.7 *Testing procedure*

The tests were carried out at a centrifuge acceleration of 60 g. The installation of a jacked pile involves many cycles of loading. In these tests, the pile base is advanced by approximately 1.5 diameters during each cycle, before the pile head is unloaded.

Each cycle consists of the following steps: (1) continuous penetration of the pile; (2) pause of penetration while the load is held approximately constant; (3) seismic tests before unloading, involving firing of the air hammers and logging of the accelerometers; (4) unloading of the pile until the pile base load is approximately zero; (5) seismic tests after the unloading of the pile base load. The next cycle then follows immediately.

During the pause in penetration of step (2), before the start of seismic tests in step (3), the soil creeps under the applied load and the pile base load gradually reduces. This reduction in stress is in general less than 15% of the value of q_c. This implies that G_0 value measured during step (3) could be up to 10% less than the value during continuous penetration.

Following the above procedures, the in situ wave velocity was monitored both before and after the unloading of the pile base of each increment of penetration. The corresponding data will be identified with a letter 'a' indicating it is obtained after the base unloading step; or with a letter 'b' indicating measurements made with the full base load mobilised.

3 RESULTS & DISCUSSION

3.1 *Pile penetration resistance*

Three tests are discussed in this paper, with the identifiers of YZ02-T2, YZ04-T1 & T3. The first test was conducted in a different sand sample from the second two tests. The pile base resistance at the end of each installation stroke, denoted q_c, is plotted against the embedment of the pile base below the soil surface in Figure 7. All data are presented in model scale units, so scaling of lengths by a factor of 60 is required to convert to equivalent prototype scale values.

For both YZ04-T1 and T3 the piles were initially buried to a depth of 45 mm during model preparation. However, at an embedment of 100 mm the q_c values converge then closely follow test YZ02-T2. This agreement suggests that both sand samples were of very similar density, as was confirmed by direct density measurements after sample preparation. Furthermore, very similar base resistance was encountered during tests YZ04-T1 and T3, indicating that the density is uniform across the plan area, within each sand sample.

3.2 G_{vh} *results*

In test YZ02-T2 a vertical array of accelerometers was placed directly underneath path of the pile base (as illustrated in Figure 4). The measured G_{0vh} values are normalized by the G_{0vh} value measured just prior to pile installation at the test g-level, giving the proportional increase in stiffness as the pile base approaches. These values of normalized G_{0vh} are plotted against the normalized distance from the pile tip, h/D, where $-h$ is the vertical distance between the pile base and the centre position between each pair of the accelerometers, and D is the pile diameter.

As is conventional in modern pile design methods, h is denoted positive upwards from the pile base (see Figure 4), so the horizontal axis of Figure 8 is negative. Data from two pairs of accelerometers are presented. Figure 8 shows results from accelerometers nos. 2 and 3, and Figure 9 shows results from accelerometers nos. 3 and 4.

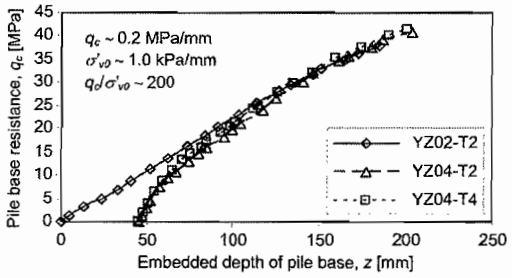

Figure 7. Pile base resistance during penetration.

A consistent trend of increasing stiffness with proximity of the pile base is observed in both tests. The normalized stiffness does not reduce to unity upon unloading. This increased stiffness that arises from the preloading of the installation phase contributes to the relatively stiffer base response of jacked piles compared to bored piles (Deeks et al. 2005). This increase can be attributed to locked-in stresses near the pile base and changes in soil fabric.

3.3 *Comparison with cavity expansion solution*

The observed increase in normalised G_0 close to the pile tip can be modelled using cavity expansion theory. If it is assumed that G_0 is proportional to the square root of the local mean effective stress p' and that $K = 1$ during penetration, thus $p' = \sigma'_v$, the profiles shown in Figure 8 and 9 can be compared with theoretical stress distributions from cavity expansion analysis.

The theoretical variation in normalized G_0 shown on Figure 8 and 9 is obtained from spherical cavity expansion analysis, which allows the radial stress below the pile, σ_r, to be calculated from the penetration resistance q_c. Normalised stiffness $G_0/G_{0,init}$ is

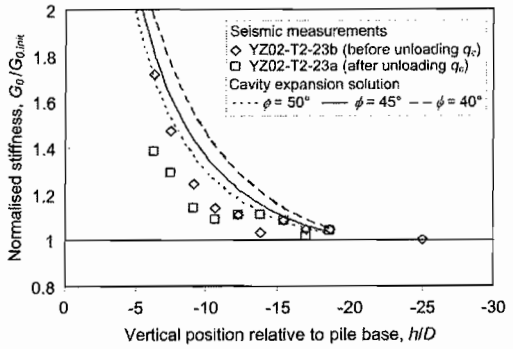

Figure 8. G_{0vh} values below pile centreline. Test YZ02, pile 2, accelerometers 2 & 3 within vertical array.

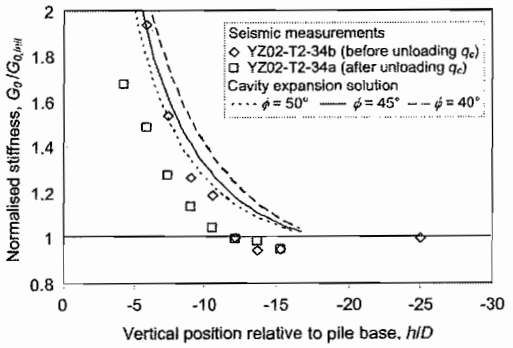

Figure 9. G_{0vh} values below pile centreline. Test YZ02, pile 2, accelerometers 3 & 4 within vertical array.

taken as the square root of the stress ratio σ_v/σ_{v0}. Since these tests were conducted in dry sand, all stresses are effective.

For a weightless frictional material obeying the Mohr-Coulomb failure criterion, the standard solution of the local radial stress at a distance -h from the centre of an expanding spherical cavity with diameter D and a cavity pressure q_c is given by Equation 1, where K_a is the active earth pressure coefficient calculated from Equation 2.

As calculated in Equation 3, the vertical stress during pile penetration, σ'_v, at a distance -h below the pile tip is assumed to be the sum of the in situ vertical stress before pile penetration, σ'_{v0}, and the cavity expansion-induced radial stress, σ'_r, found from Equation 1. The normalized stiffness $G_0/G_{0,init}$ at a depth z_{ab}, when the pile tip is located a distance -h above that point, can be calculated from the stress ratio shown in Equation 4. Substituting for q_c and K_a leads to Equation 5. The depth z_{ab} is the average vertical depth of accelerometers a and b, where a measurement of normalised G_0 can be compared with this theoretical prediction.

Theoretical stress distributions, for different angles of friction, ϕ, appropriate for very dense sand have been calculated using Equation 5 and applying the measured q_c profile from Figure 7 for test YZ02-T2. The embedded depth, z, at the mid-point between vertically-positioned accelerometers no. 2 and 3 is $z_{23} = 255$ mm and for no. 3 and 4 is $z_{34} = 215$ mm.

The theoretical distributions of normalised G_0 agree well with the measurements taken before the pile base is unloaded. The measurements tend to fall slightly below the predictions, perhaps due to a reduction in base load and hence local stress whilst the pile is held fixed during seismic testing.

$$\sigma_r = q_c\left(\frac{-2h}{D}\right)^{2(K_a-1)} \tag{1}$$

$$K_a = \frac{1-\sin\phi}{1+\sin\phi} \tag{2}$$

$$\sigma_v = \sigma_r + \sigma_{v0} \tag{3}$$

$$\frac{G_0}{G_{0,init}} = \sqrt{\frac{\sigma_v}{\sigma_{v0}}} = \sqrt{\frac{\sigma_r+\sigma_{v0}}{\sigma_{v0}}} \tag{4}$$

$$\left(\frac{G_0}{G_{0,init}}\right)^2 = \frac{q_c}{\gamma z_{ab}}\left(\frac{-2h}{D}\right)^{2(K_a-1)} + 1 \tag{5}$$

3.4 G_{hh} results

In both tests YZ-04-T1 and T3, horizontal arrays of accelerometers were employed, as illustrated in Figures 4 and 5. The centre position between accelerometers nos. 2 and 3 is offset by 40 mm (3.1 pile diameters) from the centreline of the pile shaft.

In both tests the pile base was jacked to a final base level below that of the accelerometers, hence the normalized distance, h/D, becomes positive as the pile base advances past the accelerometer positions (Figures 10 and 11).

A consistent trend of increasing small strain stiffness is seen as the pile base approaches, reflecting the increasing stress level, as also described previously for the vertical array. There is a further trend of decreasing stiffness as the pile base travels past the accelerometers, reflecting a reduction in stress around the pile shaft as the pile penetrates further.

3.5 *Friction fatigue and pile set up*

The normalised stiffness around and below the pile reduces during unloading. Below the pile the normalised stiffness remains above the in situ value after unloading indicating locked-in stress and fabric change (Figures 8 and 9).

Adjacent to the pile shaft the normalised stiffness decreases as the pile base advances beyond

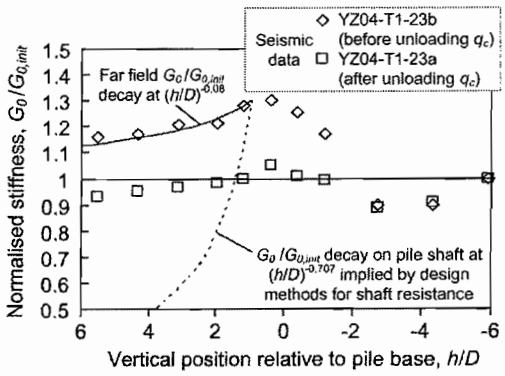

Figure 10. G_{0hh} values at 3.1D offset from pile centreline. Test YZ04, pile 1, accelerometers 2 & 3 within horizontal array.

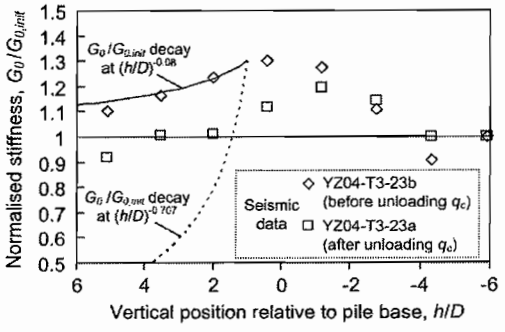

Figure 11. G_{0hh} values at 3.1D offset from pile centreline. Test YZ04, pile 3, accelerometers 2 & 3 within horizontal array.

the measurement position, and eventually turns into a deficit compared to the conditions prior to pile installation (Figures 10 and 11).

This reduction in normalised stiffness along the pile shaft is indicative of a reduction in stress acting on the pile shaft, which is a phenomenon referred to as friction fatigue (see, for example, Randolph 2003, White & Lehane 2004).

Modern pile design methods account for friction fatigue by attenuating the radial stress acting on the pile shaft by a factor $(h/D)^c$ from a maximum value close to the tip (typically at $h/D = 1$). The index c is typically -0.5 (Lehane et al. 2005). This attenuation is shown as the dotted lines on Figures 10 and 11, reduced to $(h/D)^{-0.707}$ since these figures show G_0 not stress.

The stiffness decay measured at the accelerometers offset by 3 diameters from the pile centreline is lower, and better fitted by the solid lines that have the index $c = -0.08$ for the measurements prior to base unloading.

This lower degradation of stress remote from the pile, compared to against it, is to be expected. The reduction of stress within a horizontal plane as the pile base passes can be modelled as inward relaxation. The friction ratio recorded during a cone penetration test in sand is typically 1% or less. This reduction indicates that the local stress on the pile surface drops by two orders of magnitude, passing from the base around the shoulder and onto the shaft. However, as the soil surrounding the pile moves from passive conditions (being pushed out by the advancing base) to active conditions (relaxing towards the pile shaft), the stress changes in the far field do not need to match the changes in stress acting on the pile (White et al. 2005).

However in the long term, this stress distribution may change due to creep leading to the phenomenon known as set-up, in which pile shaft resistance increases with time (see, for example, Chow et al. 1998, Zhao & White 2006). From the initial conditions of higher far field radial stress, the very low local stress on the pile surface will tend to increase, while the stress remote from the pile may decrease with time. The data shown in Figures 9 and 10 supports this model for set-up due to changes in stresses local to and remote from the pile surface.

4 CONCLUSIONS

Accelerometer arrays and air hammer vibration sources were successfully used to continuously monitor the in situ changes in shear wave velocity during the installation of jacked piles.

Consistent increases in stiffness were observed of both G_{0vh} beneath the piling position and G_{0hh} besides the pile shaft as the pile base approached.

A subsequent reduction in G_{0hh} was observed as the pile base was jacked beyond the measuring positions, to below the in situ value, indicating an annular zone of low stress close to the pile.

These measured variations in G_0 provide a valuable tool for inferring the approximate stress distribution close to the pile. The increase in stress directly below the pile base is fitted by a simple cavity expansion model. The decay in stress around the pile shaft is linked to the phenomena of friction fatigue and time-dependent set-up.

ACKNOWLEDGEMENT

Cementation Foundations Skanska provided funding for this study. We are grateful to Mr Rab Fernie and Mr Robin Wood for their support.

REFERENCES

Chow, F.C., Jardine, R.J., Brucy, F. & Nauroy, J.F. 1998. Effects of time on capacity of pipe piles in dense marine sand. *ASCE J. Geotech. & Geoenv. Engng.* 124(3): 265–276.

Deeks, A.D., White, D.J. & Bolton, M.D. 2005. The comparative performance of jacked, driven and bored piles in sand. *Proc. XVIth Int. Conf. Soil Mech. & Geotech. Engng.*, Osaka, 3:2103–2106.

Deeks, A.D. & White, D.J. 2006. Centrifuge modelling of jacked piles. *ICPMG '06*, Hong Kong.

Ghosh, B. 2004. *Behaviour of rigid foundation in layered soil during seismic liquefaction.* University of Cambridge Ph.D thesis.

Haigh, S.K. & Madabhushi, S.P.G. 2002. Dynamic centrifuge modeling of the destruction of Sodom and Gomorrah. *Int. Conf. on Physical Modelling in Geotechnics* (ICPMG), St John's, Newfoundland, Canada, July 2002: 507–512.

Lehane, B.M., Schneider, J.A. & Xu, X. 2005. The UWA-05 method for prediction of axial capacity of driven piles in sand. *Int. Symp. Frontiers in Offshore Geotechnics*: 683–689. Perth: Taylor & Francis.

Madabhushi, S.P.G., Houghton, N.E. & Haigh, S.K. 2006. A new automatic sand pourer for model preparation at University of Cambridge. *ICPMG '06*, Hong Kong.

Randolph, M.F. 2003. Science and empiricism in pile design. *Géotechnique* 53(10): 847–875.

Silva, M.F. 2005. *Numerical and physical models of rate effects in soil penetration.* Engineering Department. University of Cambridge Ph.D thesis.

White, D.J. & Lehane, B.M. 2004. Friction fatigue on displacement piles in sand. *Géotechnique* 54 (10): 645–658.

White, D.J., Schneider, J.A. & Lehane, B.M. 2005. The influence of effective area ratio on shaft friction of displacement piles in sand. *Proc. Int. Symp. on Frontiers in Offshore Geotechnics*: 741–747. Perth: Taylor & Francis.

Zhao, Y., Gafar, K., Elshafie, M.Z.E.B., Deeks, A.D., Knappett, J.A. & Madabhushi, S.P.G. 2006. Calibration and use of a new automatic sand pourer. *ICPMG '06*, Hong Kong.

Zhao, Y. & White, D.J. 2006. A model-scale investigation into 'set-up' of displacement piles in sand. *ICPMG '06*, Hong Kong.